CrossMark
click for updates

Mechanism of palladium(II) biosorption by *Providencia vermicola*

Ling Tan,[a] Haigang Dong,[b] Xinxing Liu,[a] Jia He,[a] Hang Xu[a] and Jianping Xie*[a]

The mechanism of biosorption of Pd(II) from aqueous solution onto *Providencia vermicola* biomass was elucidated from the aspects of the biosorption process, multi-scale visualization and functional groups for the first time. Kinetic, equilibrium and thermodynamic experiments revealed that the biosorption process was spontaneous, endothermic and limited by chemical reaction. The multi-scale visualization was conducted by using scanning electron microscopy coupled to energy dispersive X-ray spectroscopy (SEM-EDX), transmission electron microscopy coupled to energy dispersive X-ray spectroscopy (TEM-EDX) and atomic force microscopy (AFM). It was demonstrated that palladium ions were transformed to both the external and internal of *P. vermicola* biomass, and the morphological properties changed considerably in the nanometer range. The functional groups related to Pd(II) binding on the cell wall of *P. vermicola* were confirmed by chemical modification and characterized by Fourier transform infrared spectroscopy (FTIR) and X-ray photoelectron spectroscopy (XPS). The results showed that zero-valent palladium ions were detected in the surface of the biomass, and the most efficient functional groups were carboxylic and hydroxyl groups, followed by phosphate and amine groups.

1. Introduction

Palladium is commonly used in catalytic converters of automobiles to lower emissions of harmful pollutants, as well as in refining, electronics, dentistry, and catalysis.[1] The ability of palladium to catalyze a wide spectrum of reactions in chemical synthesis led the price of palladium to a parallel increase.[2] In general, mineral ores for the extraction of palladium contain less than 10 g t^{-1} whereas the printed circuit boards (PCBs) of personal computers and mobile phones contain 110 g t^{-1} and 280 g t^{-1} of palladium, respectively. It was reported that palladium made up around 50% of the economic value of the bare waste computer PCBs after the components were disassembled.[3] To date, hydrometallurgical processes, which include cementation, solvent extraction, ion exchange, adsorption and precipitation, account for most of the recovery of palladium from scrap. However, the recovery methods generated large quantities of secondary waste since various chemicals were used in the processes.[4,5] Hence, it is essential to develop a low-cost, eco-friendly and little secondary wastes generated system, to recover precious metals from wastewater.

In recent years, as an alternative treatment, biosorption process has become an economic and eco-friendly technology in water and wastewater industry.[6] Many biomaterials, such as bacteria, fungal, marine algae and waste activated sludge, have been investigated as biosorbents to separate and concentrate metals from wastewaters.[7,8] For example, Yan and Viraraghavan[9] reported that fungi such as *Aspergillus niger* and *Mucor rouxii* were capable of removing heavy metals from aqueous solutions. Chojnacka *et al.*[10] investigated the processes of biosorption of heavy metal ions (Cr^{3+}, Cd^{2+}, Cu^{2+}) by blue-green algae and found that *Spirulina* sp. was a very efficient biosorbent. Some industrial waste biomass, such as *Escherichia coli*[2,11] and *Corynebacterium glutamicum*,[5] were also used to recover precious metals like palladium and platinum from aqueous solution. However, the mechanism and characteristics of biosorption of various metals are bacteria dependent since the cell wall are not identical.

Providencia spp., which was used in lead, aluminium, cobalt and copper biosorption,[12,13] yet, have not been studied for palladium biosorption. The exact process of the metal uptake process, multi-scale visualization of biomass and behavior of the functional groups in the biosorption of palladium are still not clear. The objective of the present work was to investigate the biosorption processes and functional groups of *P. vermicola* biomass for recovering Pd(II) from aqueous solution. To be specific, the kinetics, equilibrium and thermodynamics characteristics of Pd(II) biosorption onto *P. vermicola* were investigated by using model fitting. Furthermore, the multi-scale visualization of blank and palladium-loaded *P. vermicola* biomass were observed using SEM-EDX, TEM-EDX and AFM. Later on, the functional groups and possible binding atoms on the cell wall were characterized by FTIR and XPS analyses. The

[a]School of Minerals Processing and Bioengineering, Central South University, Changsha 410083, China. E-mail: Xiejianping@csu.edu.cn; Fax: +86-0731-88836943; Tel: +86-0731-88836943

[b]State Key Laboratory of Advanced Technologies for Comprehensive Utilization of Platinum Metals, Kunming Institute of Precious Metals, Kunming 650106, China

Providencia vermicola biomass was chemically modified to confirm the effects of carboxyl, amine, hydroxyl, phosphate groups on the cell wall.

2. Materials and methods

2.1 Materials

Providencia vermicola was isolated from soil samples collected from YueLu Mountain (N/E: 28°10.409′/112°54.418′, Changsha, China), and the accession number of 16S ribosomal RNA gene is KX394623. The stain was grown aerobically in Luria–Bertani (LB) medium at 30 °C (under 170 rpm) for 24 h with 1% inoculation, then the *P. vermicola* cells were harvested by centrifugation at 10 000 rpm for 15 min, re-suspended in deionized water, and repelleted by centrifugation. This procedure was repeated twice, and the wet biomass was immediately used for Pd(II) biosorption.

Stock solutions of Pd(II) were prepared by dissolving PdCl$_2$ (99.0%) into 0.1 M HCl, to obtain a concentration of 500 mg L^{-1}, which were diluted as necessary.

2.2 Biosorption experiments

The biosorption experiments were carried out by contacting 0.4 g of wet biomass (equivalent to 0.075 g of dry biomass) with 50 mL of palladium solution, with an initial concentration of 200 mg L^{-1} at different pH values. The suspension was agitated at 170 rpm in a shaker at 30 ± 1 °C. After 4 h of shaking, which was sufficient to attain equilibrium, the samples were harvested and centrifuged to obtain solid–liquid separation. The Pd(II) concentration remaining in the supernatant were analyzed using an inductively coupled plasma (ICP) spectrometer (Shimadzu, ICP-7510, Japan).

Biosorption kinetic experiments were conducted using the same method as above, except that the pH was set at 2.0, 3.0 and 4.0 and the samples were collected at different time intervals to determine the time point at which biosorption equilibrium was attained sufficiently.

Biosorption equilibrium experiments were carried out by contacting 0.4 g of wet biomass with 50 mL of Pd(II) solution at temperatures of 293, 303, 313, and 323 K, respectively. The initial Pd(II) concentration was varied from 100 to 400 mg L^{-1} and pH was maintained at 4.0. After the system reached the equilibrium state, the samples were taken to determine the concentration of Pd(II).

Adsorption capacity was calculated according to the eqn (1):

$$q_t = \frac{(c_0 - c)v}{m} \tag{1}$$

where q_t (mg g^{-1}) is the adsorption capacity of biomass, v (L) indicates the volume of samples, C_0 and C (mg L^{-1}) are the initial and final concentrations of metal ions in the solution, and m (g) is the dry weight of biosorbent.

2.3 Chemical modification experiments

Portions of blank *P. vermicola* biomass were chemically treated in different ways, and then 0.4 g wet blank and modified

biomass were used for biosorption using the same methods as described. After biosorption, portion of the biomass was freeze-dried for analytical purpose.

The chemical treatment applied to the biomass were as follows:

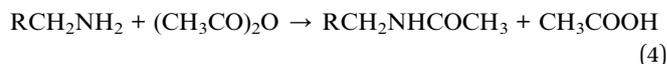Blank *P. vermicola*: conditioned biomass without modification were labeled as 'a'.

Esterification of the carboxylic groups: 5 g wet biomass was suspended in 65 mL of anhydrous methanol, and 0.6 mL of concentrated hydrochloric acid was added to the suspension. The reaction mixture was shaken on a rotary shaker for 6 h at 170 rpm. It has been shown that this treatment caused esterification of the carboxylic acids present on *Aspergillus niger*.[14] The resulted biomass samples were labeled as 'b'. The reaction occurs as follow:

$$RCOOH + CH_3OH \xrightarrow{H^+} RCOOCH_3 + H_2O \tag{2}$$

Methylation of the amines: 5 g wet biomass was contacted with 40 mL of formic acid and 20 mL of formaldehyde. The reaction mixture was shaken on an agitator at 170 rpm for 6 h. This treatment was expected to result in the methylation of amines.[15] The resulted biomass samples were labeled as 'c'. The general reaction occurs as follow:

$$RCH_2NH_2 \xrightarrow{HCHO, HCOOH} RCH_2N(CH_3)_2 + CO_2 + H_2O \tag{3}$$

Esterification of the hydroxyl groups: 5 g of raw biomass was suspended in 30 mL mixture of pyridine and acetic anhydride (12 to 88 volume ratio) and heated for 2 h at 60 °C. The treatment was widely applied for determination of hydroxyl content of carboxylic acids.[16] The biomass samples obtained were labeled as 'd'. The reaction occurs as follows:

$$RCH_2NH_2 + (CH_3CO)_2O \rightarrow RCH_2NHCOCH_3 + CH_3COOH \tag{4}$$

$$RCH_2OH + (CH_3CO)_2O \rightarrow RCH_2OCOCH_3 + CH_3COOH \tag{5}$$

Esterification of the phosphate groups: 5 g wet biomass was heated under reflux conditions with 40 mL of triethyl phosphite and 30 mL of nitromethane for 6 h. Tobin *et al.*(1990) reported that this treatment causes esterification of the phosphate groups which may be present on the biomass.[17] The resulted biomass samples were labeled as 'e'. The reaction occurs as follow:

$$3RCH_2PO_4H + (CH_3CH_2O)_3P \xrightarrow{CH_3NO_2} 3RCH_2PO_4CH_2CH_3 + H_3PO_4 \tag{6}$$
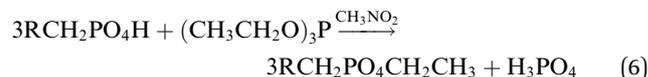
Extraction of the lipid fraction: 5 g of wet biomass was heated under reflux with 50 mL of acetone for 2.5 h.[17] The resulted biomass samples were labeled as 'f'.

2.4 Analytical methods

The samples before and after biosorption were freeze-dried for Scanning Electron Microscopy (SEM) analyses. SEM-EDX

analysis was performed on an environmental SEM (Quanta-200, FEI, UK) at 10 kV accelerating voltage. Transmission Electron Microscopy (TEM) analysis was carried out using a Tecnai G2 20 ST equipped with an energy dispersive X-ray (EDX) attachment. Prior to analysis, ultrathin sections of blank and palladium-loaded samples were cut using an ultramicrotome and then mounted on a copper TEM grid. Samples for Atomic Force Microscopy (DI Multimode V, VEECO, USA) analysis were air-dried in mica sheets overnight, and operated in tapping mode at a scan rate of 1.0 Hz using RTESP probes. For FTIR analysis, 50 mg of KBr disks containing 2% of freeze-dried powder of the each sample were prepared and then examined using a Nicolet 6700 FTIR spectrophotometer (USA). The spectra were recorded in the region of 4000–625 cm^{-1} at the resolution of 4 cm^{-1} with 32 scans. X-ray photoelectron spectroscopy (XPS) was conducted by Thermo Scientific ESCALAB 250Xi (UK) equipped with an electron flood gun and a scanning ion gun, using the Al Kα radiation (1486.6 eV) as the excitation source. The binding energy scale was calibrated with respect to adventitious carbon (C 1s).

3. Results and discussion

3.1 Study on biosorption process

3.1.1 Biosorption kinetics. Lagergren's pseudo-first-order equation, and the pseudo-second-order equation were tested to fit the experimental data (Fig. 1a). The mathematical representations of the two models are given in eqn (7) and (8), respectively.

$$\ln(q_e - q_t) = \ln q_e - k_1 t \tag{7}$$

$$\frac{t}{q_t} = \frac{1}{k_2 q_e{}^2} + \frac{t}{q_e} \tag{8}$$

where both q_e is the amount of solute sorbed at equilibrium (mg g^{-1}), q_t is the amount of solute sorbed at any time t (mg g^{-1}), k_1 is the pseudo-first-order rate constant (L min^{-1}) and k_2 is the pseudo-second-order rate constant (g (mg^{-1} min^{-1})). The experimental and predicted equilibrium uptakes, rate

constants, and corresponding correlation coefficient are summarized in Table 1.

As shown in Fig. 1a, the biosorption capacity of *P. vermicola* was significantly influenced by solution pH with the sorption capacity of 93.04 (pH 2.0), 107.15 (pH 3.0) and 115.79 (pH 4.0) respectively. And the Pd(II) biosorption was a rapid process, the adsorption reached equilibrium when the biomass contacted with Pd(II) for 180 min. The kinetic curve for Pd(II) showed rapid biosorption during the first 10 min at pH 4, with a Pd(II) removal efficiency of 80%.

The correlation coefficients in the pseudo-first-order model were in the range of 0.70–0.76 (Table 1), but the calculated q_e were not consistent with the experimental q_e values, since the pseudo-first-order model only represented kinetic experiment data of the rapid initial phase.[2] Conversely, the pseudo-second-order model, based on the assumption that the rate-limiting step may be chemical sorption involving valency forces through sharing or exchange of electrons between sorbent and sorbate, provided the best correlation of the data.[18,19] On the other hand, the rate constant calculated from both pseudo-first-order (k_1) and pseudo-second-order (k_2) at pH 2.0 and 3.0 were only 0.285, 0.005 and 0.256, 0.004, much lower than 0.384 and 0.006 at pH 4.0, which meant that the adsorption process was significantly hindered under low pH.

In contrast to pseudo-second-order model, the intraparticle diffusion model (eqn (9)) may provide a more comprehensive view of adsorption.

$$q_t = k_i t^{0.5} + C \tag{9}$$

where k_i is the intraparticle diffusion rate constant (mg g^{-1} min$^{-0.5}$), which can be calculated from the slop of the linear plots of q_t *versus* $t^{0.5}$.

According to Weber and Morris, if the rate-limiting step is intraparticle diffusion, a plot of solute sorbed against the square root of the contact time should yield a straight line passing through the origin.[20] If the plot shows multi-linearity, it indicates that further complexity exists in the adsorption process.[21] Multi-linearity was clearly observed over the whole time range as shown in Fig. 1b, indicating that two steps
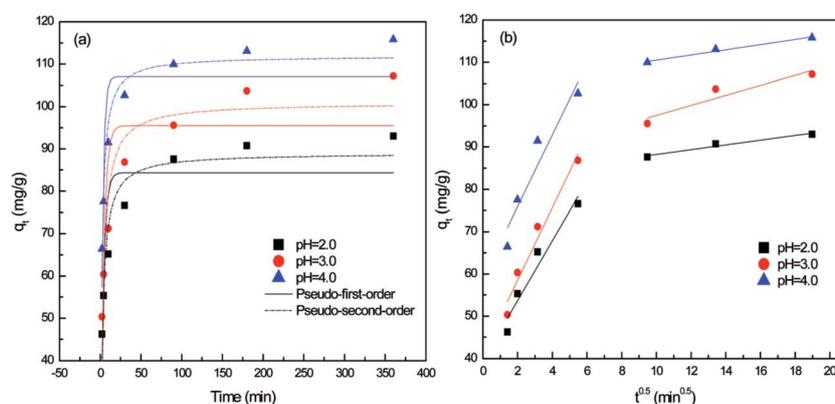

Fig. 1 Non-linear kinetic fits of for *P. vermicola* biomass at different pH. (a) Pseudo-first-order and pseudo-second-order model; (b) intraparticle diffusion model.

Table 1 Kinetic parameters of pseudo-first-order, pseudo-second-order model and intraparticle diffusion model for *P. vermicola* biomass at different pH

Fitting models	Stages	Parameters	pH = 2.0	pH = 3.0	pH = 4.0
Pseudo-first-order model		Experimental q_e (mg g^{-1})	93.038	107.734	115.791
		Predicted q_e (mg g^{-1})	84.332	95.493	107.059
		K_1 (L min^{-1})	0.285	0.256	0.384
		R^2	0.713	0.706	0.755
Pseudo-second-order model		Predicted q_e (mg g^{-1})	89.000	100.929	111.934
		K_2 (g mg^{-1} min^{-1})	0.005	0.004	0.006
		R^2	0.916	0.905	0.953
Intraparticle diffusion model	First stage	C (mg g^{-1})	39.537	41.362	59.027
		K_{i1} (mg g^{-1} min$^{-0.5}$)	7.068	8.569	8.456
		R^2	0.918	0.953	0.875
	Second stage	C (mg g^{-1})	82.579	85.637	104.421
		K_{i2} (mg g^{-1} min$^{-0.5}$)	0.564	1.183	0.609
		R^2	0.928	0.788	0.962

governed adsorption rather than one. The first sharper stage was film physical diffusion, in which Pd(II) were transported onto the external surface of biomass. The second stage described the gradual biosorption, where metals were sorbed on the interior of the biomass and intraparticle diffusion was rate-limiting. As reflected in Table 1, the intraparticle diffusion rate constant in first stage was higher than that in later stage ($k_{i1} > k_{i2}$), which were observed in pH 2.0, 3.0 and 4.0. It meant that the exterior surface adsorption was an instantaneous diffusion process. When exterior surface reached saturation, palladium ions entered the biomass on the second stage with increased diffusion resistance, resulting in a decrease of diffusion rates (k_{i2}). As Min[22,23] reported, the adsorption was controlled by two steps or more, including boundary layer or external diffusion, pore diffusion, surface diffusion and adsorption onto the pore surface, or a combination of several steps, of which the intra-particle diffusion step was the most rate-limiting procedure. The multi-linearity in the shape of the intraparticle diffusion plot had also been observed by Ofomaja in the biosorption of lead, methylene blue and methyl violet onto mansonia wood sawdust.[21,24]

3.1.2 Biosorption equilibrium. The biosorption isotherm models describe the correlation between the mass of solute sorbed per unit mass of sorbent at equilibrium. The biosorption isotherms were calculated using two different isotherms models including the Langmuir, and Freundlich isotherms (Fig. 2).

The saturated monolayer isotherm model can be represented as Langmuir, and the mathematical representation is given in eqn (10).

$$q_e = \frac{q_m K_L C_e}{1 + K_L C_e} \quad (10)$$

where q_e is the amount of metal ion sorbed (mg g^{-1}); q_m is the saturated sorption capacity (mg g^{-1}); K_L is biosorption equilibrium constant (L mg^{-1}) and C_e is the equilibrium concentration (mg L^{-1}) remained in the solution.

The empirical Freundlich isotherm model, based on sorption on heterogeneous surface, is given by eqn (11).

$$q_e = K_F C_e^{1/n} \quad (11)$$

where q_e is the amount of metal ion sorbed (mg g^{-1}); C_e is the equilibrium concentration (mg L^{-1}) remained in the solution; K_F and $1/n$ are the Freundlich constants characteristics of the system, indicating the sorption capacity and sorption intensity, respectively; and n is the heterogeneity factor which is also known as Freundlich coefficient.

In present study, correlation coefficients (R^2) showed that the Langmuir model fitted the Pd(II) biosorption data better than the Freundlich model, implying a monolayer adsorption trend.[25] The isotherm data calculated from Freundlich isotherm (Table 2) revealed that the $1/n$ values for Pd(II) at 293, 303, 313 and 323 K were 0.281, 0.268, 0.278 and 0.307, respectively. The value of $1/n$ range between 0 and 1 further confirmed the favorable adsorption for palladium ions. Furthermore, the isotherms with n values greater than unity were classified as L-type isotherms which showed that there was high affinity between adsorbate and adsorbent surface.[23,26] The maximum biosorption capacity calculated from Langmuir isotherm presented in Table 2 was 196.806 mg g^{-1} for the biosorption of Pd(II). This biosorption capacity is higher than
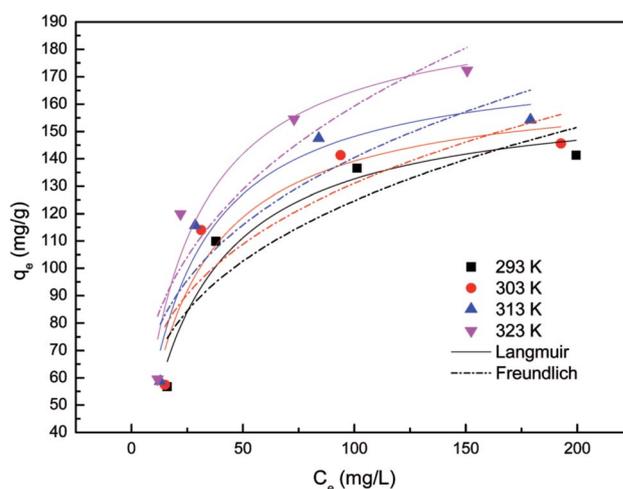

Fig. 2 Non-linear fits of Langmuir and Freundlich isotherm models for *P. vermicola* biomass.

Table 2 Isothermic parameters of Langmuir and Freundlich models for *P. vermicola* biomass

	T (K)			
Isotherm	293	303	313	323
Langmuir				
q_m (mg g^{-1})	164.313	168.101	177.659	196.806
K_L (L mg^{-1})	0.042	0.048	0.050	0.052
r^2	0.930	0.882	0.923	0.907
Freundlich				
$1/n$	0.281	0.268	0.278	0.307
K_F (mg g^{-1}) (L mg^{-1})$^{1/n}$	34.144	38.142	39.073	38.791
r^2	0.743	0.681	0.734	0.779

those reported for *Racomitrium lanuginosum*[27] and *Escherichia coli*.[28]

3.1.3 Biosorption thermodynamics. Thermodynamic considerations of a biosorption process are necessary to conclude whether the process is spontaneous or not. The Gibbs free energy (ΔG^0) change, is an indication of spontaneity of a chemical reaction and therefore is an important criterion for spontaneity. Also, both enthalpy (ΔH^0) and entropy (ΔS^0) factors must be considered to determine the Gibbs free energy of the process. These parameters were calculated according to following equations.

$$\Delta G^0 = -RT \ln K_L \quad (12)$$

$$\Delta G^0 = \Delta H^0 - T\Delta S^0 \quad (13)$$

where ΔG^0 is the standard Gibbs free energy change (J), R the universal gas constant, 8.314 J mol^{-1} K^{-1}, T is absolute temperature (K), K_L is the equilibrium constant of Langmuir, ΔH^0 is the enthalpy change, and ΔS^0 is the entropy change.

The Gibbs free energy change (ΔG^0) and temperature (T) showed a linear relationship (Fig. 3). The values of ΔH^0 and ΔS^0 were determined from the slope and intercept of the plot. Gibbs
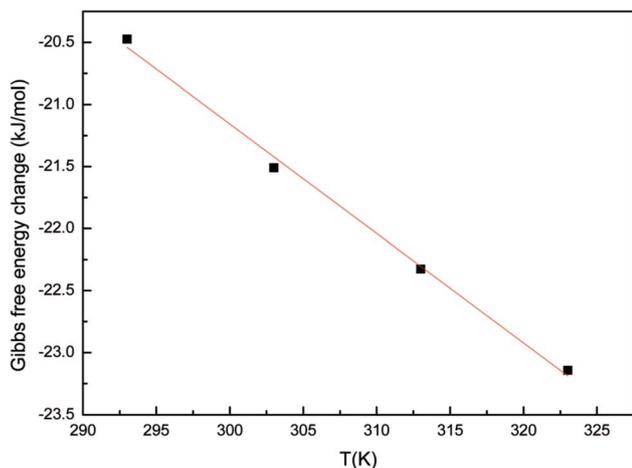

Fig. 3 Plot of ΔG^0 *vs.* T for the estimation of thermodynamic parameters for *P. vermicola* biomass.

free energy change (ΔG^0) were −20.47, −21.51, −22.33, −23.14 kJ mol^{-1} for Pd(II) biosorption at 293, 303, 313 and 323 K, respectively. The enthalpy change (ΔH^0) and the entropy change (ΔS^0) for the biosorption process were 5.319 kJ mol^{-1} and 0.088 J mol^{-1} K^{-1}, respectively. Negative values of ΔG^0 confirmed the feasibility of the process and the spontaneous nature of biosorption with a high preference for palladium on *P. vermicola*. The value of ΔH^0 was positive, indicating that the biosorption reaction was endothermic. In addition, negative enthalpy (ΔH^0) was characteristic of metal ions coordination with amino and sulfhydryl groups, whereas coordination with oxygenous functional groups resulted in small positive enthalpies.[29,30] The result implied that the Pd(II) might be bound to the oxygen atoms from active groups (*e.g.* –COOH and –OH) on the cell wall in this case. The positive value of ΔS^0 reflected the affinity of *P. vermicola* for palladium ions and suggested some structural changes during the biosorption process. Further, positive value of ΔS^0 showed increasing randomness at the solid/liquid interface during the biosorption of Pd(II) onto *P. vermicola*.[25] Mehrorang *et al.* reported that the biosorption of Co^{2+}, Cu^{2+}, Ni^{2+}, Pb^{2+} and Zn^{2+} ions onto *Trichoderma reesei* biomass was feasible, spontaneous and endothermic at the optimized conditions.[31] Also, during the process of removal of Cd(II) and Cu(II) from aqueous solution by magnesium chloride-modified *Lentinula edodes*, the thermodynamic parameters determined indicated that the biosorption process was endothermic and spontaneous.[32]

3.2 Multi-scale visualization of *Providencia vermicola* biomass

3.2.1 SEM-EDX analysis. *P. vermicola* cells (palladium-loaded biomass) were observed using SEM-EDX after exposure to an aqueous PdCl$_2$ solution. Since there was no obvious morphology difference between blank and palladium-loaded biomass (data not shown), the palladium-loaded biomass (Fig. 4a) was subjected to EDX analysis. Fig. 4b showed a representative energy dispersive spectrum of palladium-loaded biomass of *P. vermicola*, specific peaks for palladium and chloride were detected with carbon, nitrogen, oxygen, phosphorus and sulfur. The later elements were derived from the *P. vermicola* cell, whereas palladium and chloride were traces of palladium complexes sorbed on the surface of *P. vermicola* biomass. To further confirm the location of the palladium deposition, the EDX maps of palladium and chloride were obtained (Fig. 4c and d). As a result, palladium and chloride were present all everywhere just like the distribution of *P. vermicola* cells in Fig. 4a, indicating the uniform distribution of palladium complexes on the biomass. Table 3 summarized the surface elemental composition of section 1 of Fig. 4a. It revealed that the wt% of Pd and Cl reached 18.40% and 4.32%, respectively. Compared to other researches, it was observed from SEM pictures that the surface of the biomass becomes rougher and shows the presence of new shiny bulky particles over the surface of the biomass saturated with Cr(VI) than in case of before adsorption.[33] When using *Aspergillus niger* for removal of chromium(VI), the SEM-EDX analyses revealed that chromium was
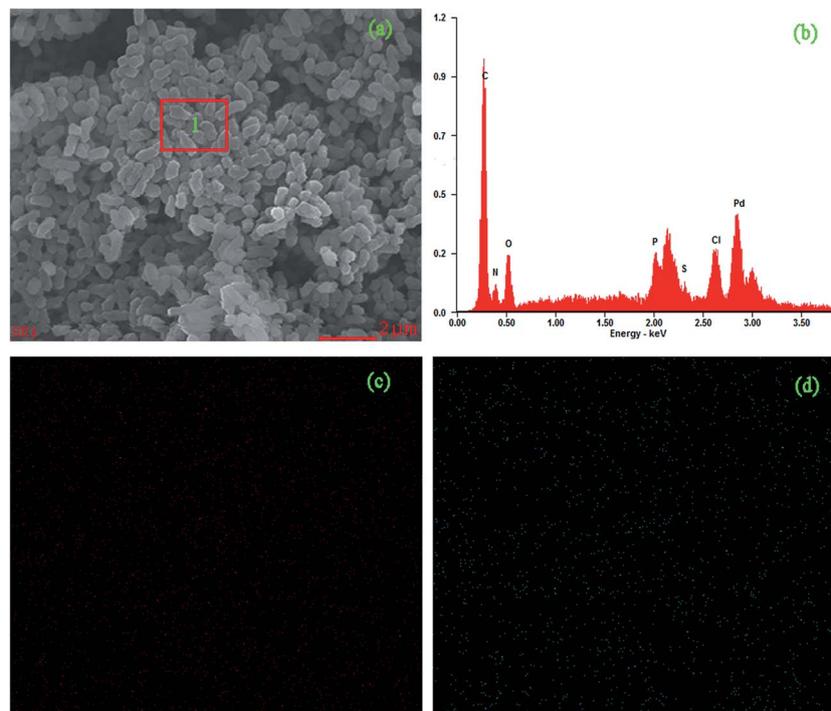
Fig. 4 SEM-EDX analyses of palladium-loaded biomass after exposure to 200 mg g^{-1} aqueous PdCl$_2$ solution for 3 h. (a) Micrograph of palladium-loaded biomass; (b) spot profile EDX spectrum recorded from region 1; (c) X-ray maps of palladium from 'a' obtained by EDX analysis; (d) X-ray maps of chloride from 'a' obtained by EDX analysis.

uniformly bound to the fungal mycelium and a higher chromate absorption together with flocculation in mycelium was observed.[34]

3.2.2 TEM-EDX analysis. TEM-EDX was used to investigate whether palladium ions presented in the internal of cells or not. As shown in Fig. 5a and b, the average dimension of these cells was about 2.0 μm long and 0.8 μm wide, but the difference between images of blank and palladium-loaded *P. vermicola* was invisible similar to results obtained by SEM. Therefore, samples were analyzed by energy dispersive X-ray (EDX) together with TEM, allowing to verify the presence of palladium in the cells. The EDX spectra derived from blank biomass indicated that it consisted of carbon, oxygen, phosphorus (Fig. 5c). The copper peak was from the grid used to support the sections, and the lead peak originated from the Pb(CH$_3$COO)$_2$ used the cell pellet staining. Furthermore, EDX spectra (Fig. 5d) originating from palladium-loaded biomass exhibited the characteristic peak of

palladium, which confirmed the presence of palladium ions in the internal of cells. Since the SEM-EDX and TEM-EDX confirmed the existence of palladium ions in both external and internal of *P. vermicola* biomass. The process involving the binding of palladium ions could occur as follows: firstly, the palladium bound to functional groups by electrostatic interaction; it was subsequently transported into the cytoplasm through different layers (peptidoglycan, teichoic acids) of the cell wall and cytoplasmic membrane, and gradually formed complexes.[35] Likewise, by using HAADF-STEM-EDX analysis, Omajali *et al.*[36] proved that intracellular palladium nanoparticles were formed in *B. benzeovorans* with H$_2$ or formate as electron donors. Koshiro *et al.* reported that the rhodium nanoparticles were deposited intracellularly in *Shewanella algae* by comparing the biogenic nanoparticles in the TEM image and the X-ray map for rhodium.[37]

3.2.3 AFM analysis. Visualizing microbial surface at higher resolution, preferably in the nanometer level, is crucial to understand the structure changes after exposing in palladium solution. Although SEM and TEM images showed no big morphological difference between blank and palladium-loaded biomass, AFM results showed that the surface of the palladium-loaded biomass was clearly different from that of the blank biomass (Fig. 6). The blank *P. vermicola* seemed to huddle together with clear boundaries between each other (Fig. 6a), and the phase image showed some wrinkles (Fig. 6b) which might because of the extrusion force. In addition, their surface had a relative smooth appearance and preserved the integrity of cell structure including the shape and size. However, the

Table 3 Surface elemental composition of palladium-loaded biomass by SEM-EDX analysis

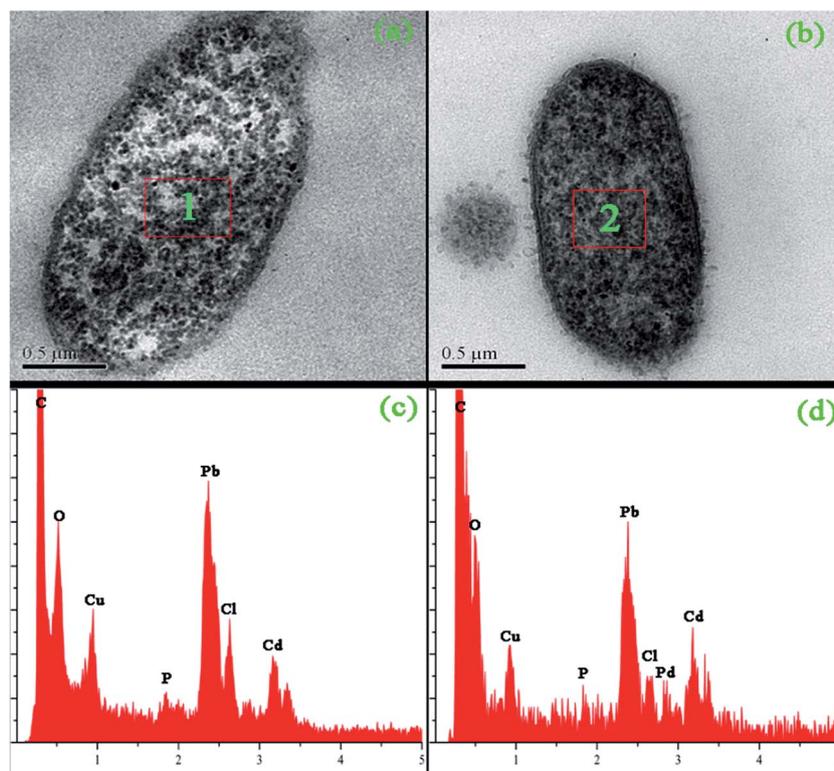| Element	Wt%	At%
C	45.55	62.50
N	13.55	15.94
O	14.14	14.56
P	02.95	01.57
S	01.09	00.56
Cl	04.32	02.01
Pd	18.40	02.85

Fig. 5 TEM analyses of blank and palladium-loaded biomass after exposure to 200 mg g^{-1} aqueous PdCl$_2$ solution for 3 h. (a) TEM images of thin section of blank biomass; (b) TEM images of thin section of palladium-loaded biomass; (c) spot profile EDX spectrum recorded from region 1; (d) spot profile EDX spectrum recorded from region 2.

morphological change of palladium-loaded biomass was obvious, the change included the shape, adhesion and roughness properties. The palladium-loaded biomass became more roughened in the surface with the cell dimension changed (Fig. 6c and d). A great number of granules were appeared in the surface of palladium-loaded *P. vermicola*, and the boundaries between cells became ambiguous. Furthermore, unlike blank biomass that laid flat on the mica plate, the palladium-loaded biomass had a strong tendency toward formation of large clumps, which upon examination appeared to be both bacteria and nanoparticle aggregates coagulated together. This superficial change was attributed to the interactions between palladium ions and the surface of *P. vermicola* surface, the results were in accordance with the recent findings of Jiyeong Park[2] and Stoimenov.[38] In addition, the morphological changes of Pb^{2+} ion-exposed *Bacillus cereus* cells in the biosorption processes, including the size, shape and adhesive properties of the bacteria were also observed.[39]

3.3 Functional groups characterization

3.3.1 FTIR analysis. The cell walls of bacteria consist of several polymers and macromolecules, which have carboxyl, amide, hydroxyl and phosphate functional groups. From the FTIR adsorption peaks of *P. vermicola* biomass (Fig. 7), a number of absorption peaks and the complex nature of the biomass were examined and displayed. The adsorption range of 3200–3600 cm^{-1} represented N–H asymmetric stretching of the

amines and O–H bond of the hydroxyl groups on the biomass surface.[2,11,28] In this case, the intensity of peak valley at 3301 cm^{-1} in blank *P. vermicola* biomass was deepened and shifted after sorbing palladium, suggesting the N–H and O–H involvement to palladium adsorption. The absorption peaks at 1653 and 1541 cm^{-1} were attributed to the amide I (C=O) and amide II (N–H) bonds of the protein peptide bonds.[2,35] A strong bond at 1455 cm^{-1} was characteristic of –CH$_2$ scissoring motion and –CH$_3$ antisymmetrical bending vibration, which were common in peptidoglycan, LPS, and phospholipids.[40,41] The symmetric stretching of COO$^-$ vibration appeared around 1396 cm^{-1},[2,35,42] which had shifted to 1386 cm^{-1}, demonstrated that carboxyl was a contributor in the sorption of Pd(II). Another strong bond around 1236 cm^{-1} was caused by functional groups, such as P=O of polysaccharides and phospholipids inside the cell wall.[41,43] The spectrum displayed adsorption peak at 1078 cm^{-1} moved to a lower frequency, which was related to the phosphate groups (P=O and P–O of the C–PO$_3{}^{2-}$ moiety).[2,28,35] In contrast to the spectrum of blank biomass, the FTIR spectrum of palladium-loaded biomass showed that the peaks expected at 3301, 1541, 1396, 1236 and 1078 cm^{-1} had shifted to 3307, 1538, 1386, 1230, and 1068, respectively (Fig. 7). These shifts indicated that N–H, O–H, –COOH, P=O and P–O, might be the predominant contributors in the sorption of Pd(II). On the other hand, since there was no big difference between the spectra of blank *P. vermicola* biomass and palladium-loaded biomass, especially for the main characteristic absorption peak (amide I
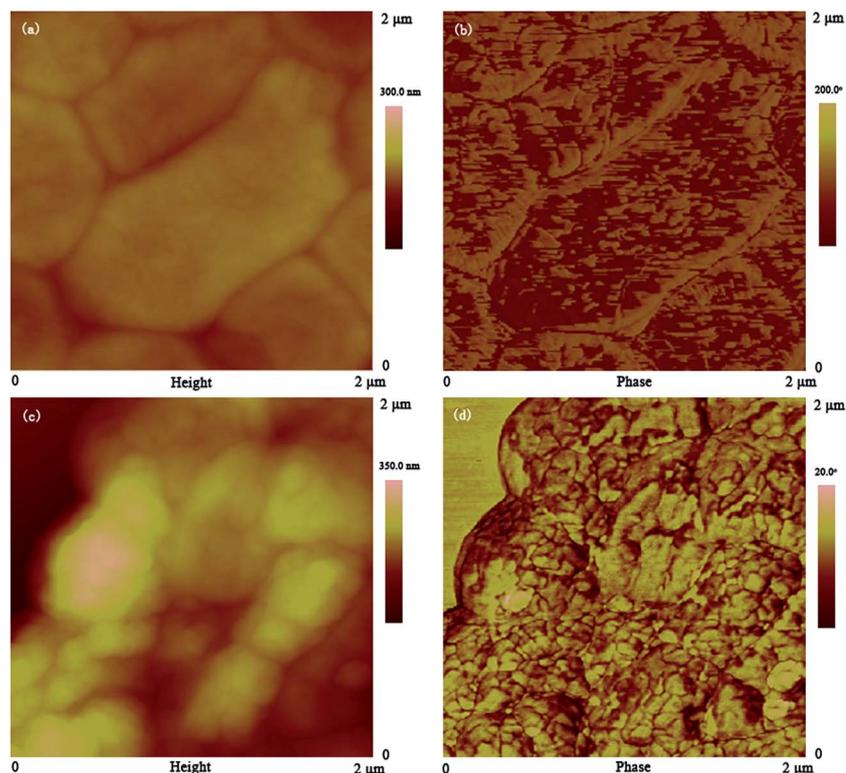
Fig. 6 AFM analyses of blank and palladium-loaded biomass after exposure to 200 mg g^{-1} aqueous PdCl$_2$ solution for 3 h. (a) AFM height images of blank biomass; (b) AFM phase images of blank biomass; (c) AFM height images of palladium-loaded biomass; (d) AFM phase images of palladium-loaded biomass.

and amide II), indicating the structure and composition of *P. vermicola* was not destroyed after adsorbing palladium.

3.3.2 XPS analysis. The automatic environment changes before and after biosorption were characterized using XPS analysis. Fig. 8a showed that the wide scan spectrum comprised mainly carbon, nitrogen and oxygen. After palladium biosorption, a new peak corresponded to Pd 3d was clearly appeared. The Pd 3d signal of palladium-loaded biomass (Fig. 8b) was fitted to two pairs of doublets with a spin–orbit separation of 5.3 eV. It was reported that Pd 3d3/2 (341.2 eV), Pd 3d5/2 (335.9 eV) and Pd 3d3/2 (337.6 eV), Pd 3d5/2 (342.8 eV) could be assigned to Pd(0) and Pd(II), respectively.[44–46] In this study, two signals (341.2 eV and 335.9 eV) corresponding to Pd(0) (3d3/2 and 3d3/2) were detected, confirming the presence of elemental palladium. There were two possibilities that the elemental palladium stemmed from, first, Pd(II) anchored on the surface of *P. vermicola* was reduced to Pd(0); second, the Pd(II) was reduced inside *P. vermicola* and released with the disruption of cells.

The O 1s signal (Fig. 8c) in blank cells fitted to three different peaks (531.3, 532.3 and 533.1 eV), which could be attributed to carbonyl oxygen in amide and carboxyl, oxygen atoms in hydroxyls or ethers and oxygen atoms in esters, respectively.[35] A minor shift of the peaks at 531.3 and 532.3 eV to 531.4 and 532.4 eV indicated the role of carboxyl and hydroxyl groups in palladium binding. This result was also consistent with the negative enthalpy (ΔH^0) in biosorption thermodynamics, which

implied the Pd(II) might be bound to the oxygen atoms from active groups (*e.g.* –COOH and –OH) on the cell wall.

Deconvolution of the C 1s spectra (Fig. 8d) could generate four peaks at 284.5, 285.0, 286.1, and 287.9, which correspond to carbon making a single bond with carbon (C–C at 284.5 eV), carbon making a single bond with hydrogen (C–H at 285.0 eV),
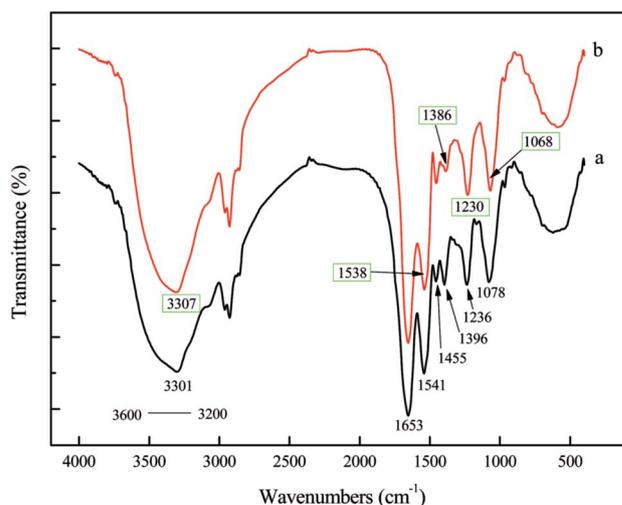

Fig. 7 FTIR spectrum of blank and palladium-loaded biomass after exposure to 200 mg g^{-1} aqueous PdCl$_2$ solution for 3 h. (a) Blank biomass; (b) palladium-loaded biomass.
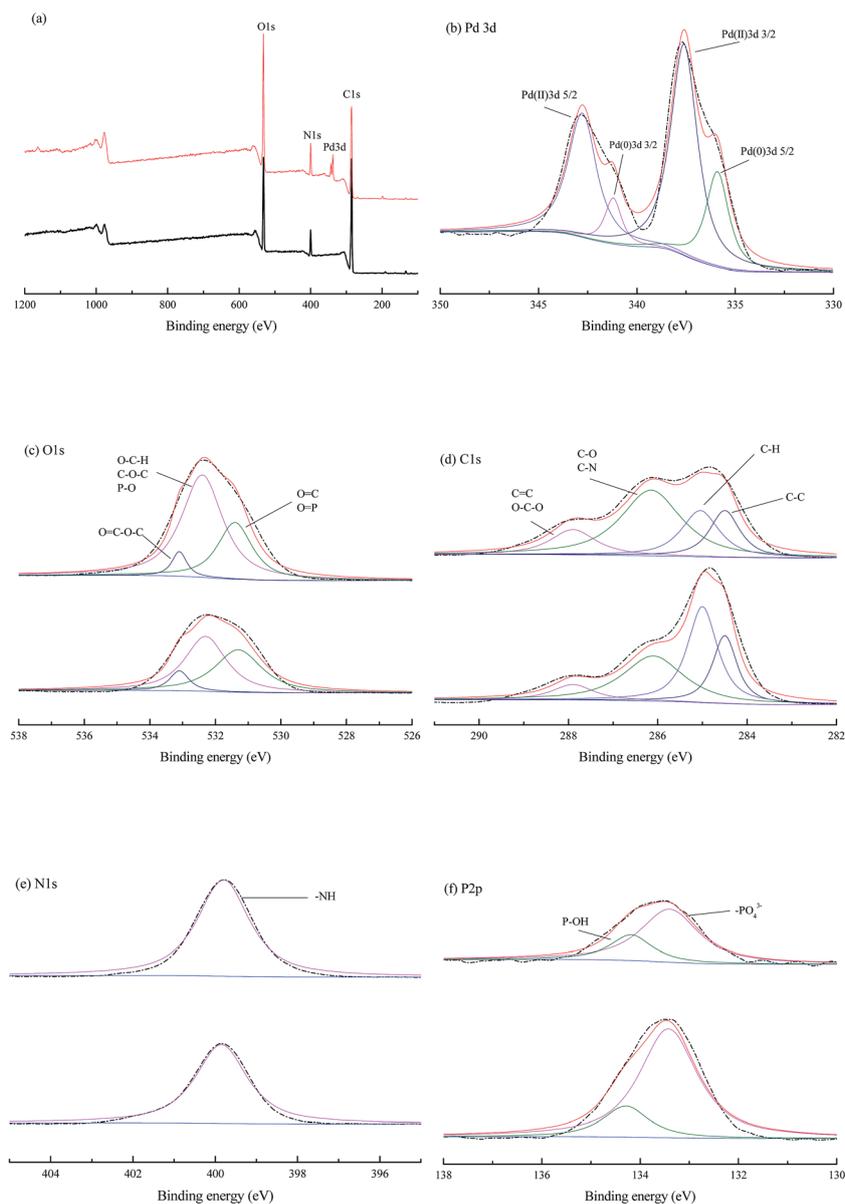
Fig. 8   X-ray photoelectron binding energy curves of blank (up) and palladium-loaded (down) biomass after exposure to 200 mg g^{-1} aqueous PdCl$_2$ solution for 3 h. (a) Total survey scans; (b) Pd 3d spectra; (c) O 1s spectra; (d) C 1s spectra; (e) N 1s spectra; (f) P 2p spectra.

carbon bound to oxygen or nitrogen (C–O, C–N, at 286.1 eV, attributed to alcohol, amine or amide), carbon making two single bonds or one double bond with oxygen (C–O–C, C═O at 287.9, attributed to hemiacetal, acetal, amide and carboxylate).[35,47] The carbon only bounded to carbon and hydrogen C–(C, H), might derive from lipids or the side chains of amino acids. Acetal or hemiacetal could arise from polysaccharides and sugar moieties.[29] Further, the amide was expected to represent peptidic bonds, and carboxylate and carboxyl functional groups may be due to proteins and possibly uronic acids.[48]

The XPS spectrum (Fig. 8e) showed a single N 1s peak at 399.8 eV in both blank and palladium-loaded *P. vermicola*, attributable to nitrogen in –NH$_2$ groups,[2,11] which implied

a single chemical environment in *P. vermicola*. The fitted P 2p envelope (Fig. 8f) indicated the presence of two components, positions of 133.3 and 134.2 eV, which corresponded to the P 2p3/2 and P 2p1/2 states of phosphorus in *P. vermicola*. The P 2p peak locating at 133.3 eV could be deconvoluted into contributions from the P(v) oxidation state, corresponding to the –[PO$_4$]$^{3-}$, while 134.2 eV corresponding to P–OH.[49,50]

In summary, both Pd(0) and Pd(ii) were detected on the surface of *P. vermicola* biomass, and O atom was related to the biosorption of palladium ions. The peaks of C, N, P between blank and palladium-loaded *P. vermicola* remained unchanged, but the peak area ratio of binding energy peaks was different, which implied the possible sorption capabilities of those atoms. When comes to the biosorption of uranium by a novel

Streptomyces sporoverrucosus dwc-3, the XPS and FT-IR analysis suggested that the absorbed uranium was bound to amino, phosphate and carboxyl groups of the cells.[35]

3.4 Functional groups confirmation

3.4.1 Chemical modification of *P. vermicola* biomass. The effects of chemical treatment on the functional groups could be evaluated from the differences among the spectrums. The curve in Fig. 9b portrayed the FTIR spectrum of *P. vermicola* treated

with methanol and hydrochloric acid, which resulted in the esterification of carboxyl groups. When comparing Fig. 9a with b, the carboxyl related peaks at wave number of 1653 cm^{-1} and 1396 cm^{-1} in blank biomass (Fig. 9a), which represented C=O in amide I and COO$^-$ respectively, changed significantly. Specifically, the former shifted to 1646 cm^{-1}, and the trough observed at 1396 cm^{-1} almost disappeared. In addition, the methanol-treated biomass clearly displayed shifts of O–H bond located at 3301 cm^{-1} because the addition of extra –OH in methanol.
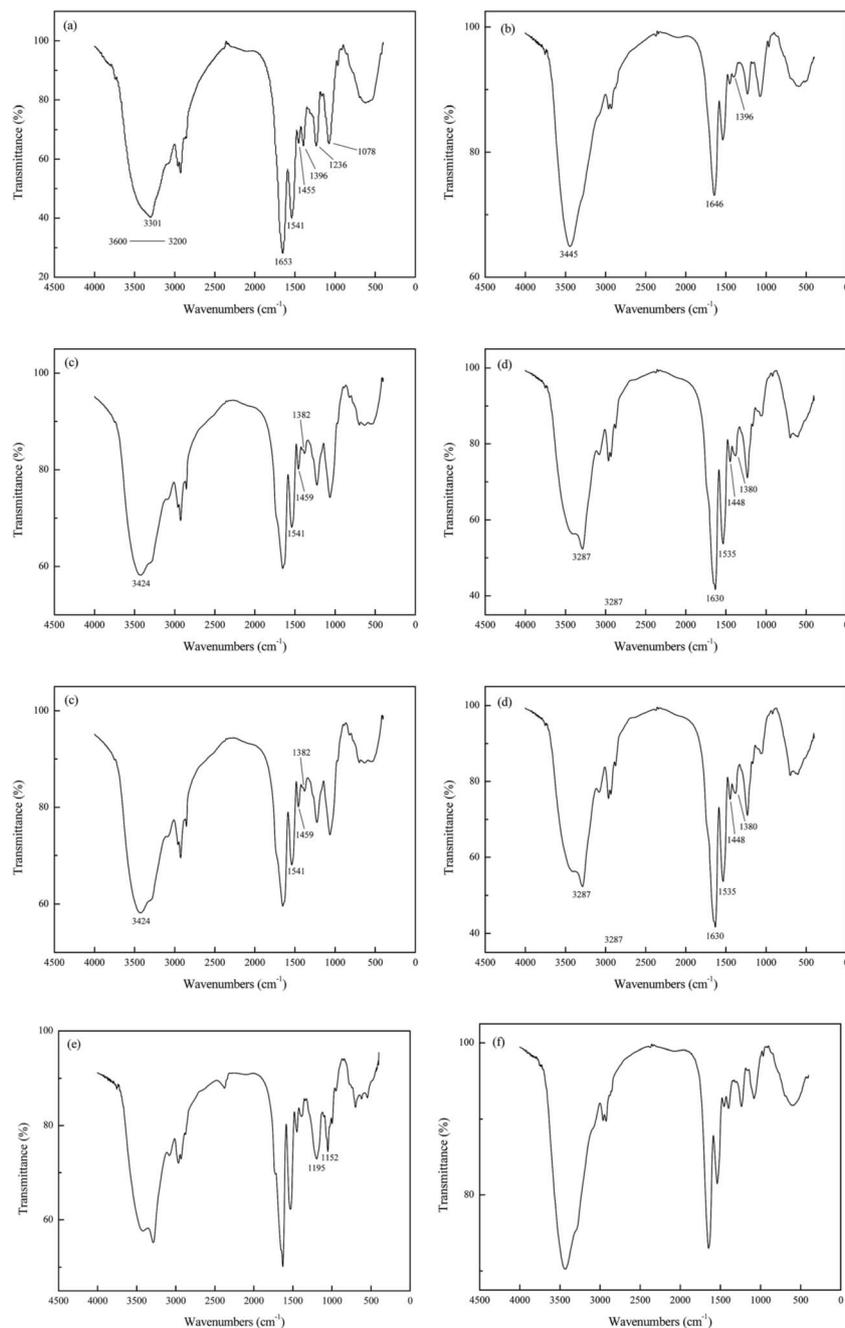

Fig. 9 FTIR spectra of blank and chemically modified biomass. (a) Blank biomass, (b) biomass treated with methanol and hydrochloric acid, (c) biomass treated with formic acid and formaldehyde, (d) biomass treated with acetic anhydride and pyridine, (e) biomass treated with triethyl phosphite and nitromethane, (f) biomass treated with acetone.

Treatment of biomass with formic acid and formaldehyde gave rise to the methylation of amino groups as depicted in Fig. 9c. The peak at 3301 cm^{-1} (N–H and O–H bond) shifted to 3424 cm^{-1}, which suggested certain changes had been happened to the amino groups presented in the biomass. The N–H bond at wave of 1541 cm^{-1} remained the same, indicating the major components and structure of biomass remained intact. On the other hand, the peak at 1396 cm^{-1} represented COO$^-$ shifted to 1382 cm^{-1}, implying the modification not only changed the amide groups on the biomass but also the carboxyl groups. Furthermore, a change in the peak 1455 cm^{-1} in the spectrum of the treated sample confirmed the change in methyl as reaction (3) showed.

The Fig. 9d shows the FTIR spectrum of biomass treated with acetic anhydride and pyridine which could esterify the hydroxyl groups and the amines simultaneously. The hydroxyl and amine peaks at 3301 cm^{-1} represented N–H asymmetric stretching of the amines and O–H bond of the hydroxyl groups, and 1541 cm^{-1} represented N–H bonds in amide II. Those two peaks shifted to 3287 cm^{-1} and 1535 cm^{-1} respectively, verifying the modification of function group in biomass. Likewise, the peaks at 1653 cm^{-1}, 1455 cm^{-1} and 1396 cm^{-1} moved to 1630 cm^{-1}, 1448 cm^{-1} and 1380 cm^{-1} respectively, which might due to the residual acetic anhydride and formation of amino and acetic acid as reaction (4) showed.

The Fig. 9e displayed the FTIR spectrum of biomass treated with triethyl phosphite and nitromethane which could esterify the phosphate groups. The peaks at wave number of 1236 cm^{-1} and 1078 cm^{-1} moved to 1195 cm^{-1} and 1052 cm^{-1} with a very different spectral intensity in this chemically modified biomass.

As shown in Fig. 9f, the wave numbers of peaks in biomass treated with acetone remained a relative unchanged positions, which indicated the extraction of lipid fraction did not affect the structure and function groups of *P. vermicola*.
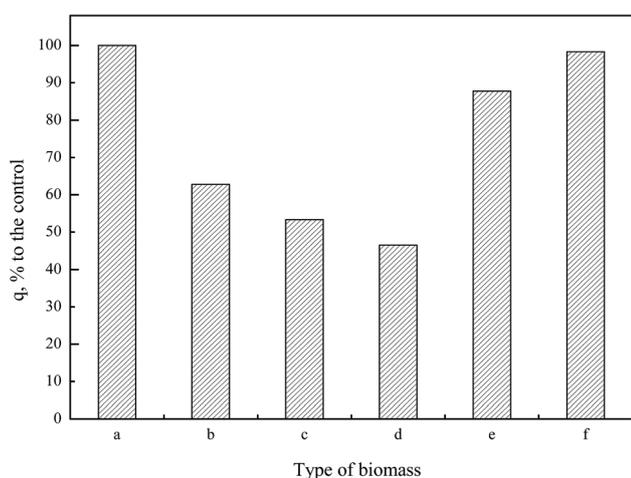

Fig. 10 Palladium biosorption efficiency of blank and chemically modified biomass. (a) Blank biomass, (b) biomass treated with methanol and hydrochloric acid, (c) biomass treated with formic acid and formaldehyde, (d) biomass treated with acetic anhydride and pyridine, (e) biomass treated with triethyl phosphite and nitromethane, (f) biomass treated with acetone.

In summary, Fig. 9 showed a strong evidence of successful chemical modification on blank *P. vermicola*. Those modified biomass could be used to verify the effects of carboxyl, amine, hydroxyl, phosphate and lipid groups on the surface of cell wall.

3.4.2 Experimental confirmation of functional groups. The modification of those function groups definitely affected the capacity of *P. vermicola* biomass. Results of metal binding studies for blank and chemically treated *P. vermicola* biomass were shown in Fig. 10. Biosorption of palladium was observed to be severely inhibited (about 40% reduction of uptake) when carboxylic groups was esterified (b), indicating the important role of carboxylic groups in the biosorption of Pd(II). Since the formaldehyde used for methylation of amines could also replace the H atoms present on COOH, the effect of the formic acid-formaldehyde treatment (c) would indicate the contribution of amino and carboxyl groups.[14] By combining the results from treatments b and c, it could be concluded that Pd(II) biosorption was more sensitive to the modifications of the carboxyl groups than that of the amine groups, where the observed reduction of the uptake was found to be about 40% and 10% respectively. The reduction of the uptake caused by modification of hydroxyl and amine groups (d) was about 50%. By eliminating the contribution of amine groups (about 10%), the contribution of hydroxyl groups in biosorption was about 40%, which played a comparable role as carboxylic groups. More than 10% decrease in the palladium uptake was observed in sample treated with nitromethane and triethyl phosphite (e), suggesting phosphate groups represented the fraction of reactive groups in the surface of *P. vermicola*. It was expected that extraction of the lipid fraction might alter the uptake level of palladium. However, the results (f) treatment exhibited a very slight decrease (about 2%) in adsorption capacity, implying that any biomass constituents extracted in these treatments did not contribute to the uptake of palladium.

In Pd(II) biosorption, the spectral analysis and biosorption test disclosed that the most efficient functional group on the cell wall of *P. vermicola* were carboxylic and hydroxyl groups which was followed by phosphate and amine groups. The effect of chemical modification on metal uptake capacity appeared to be biomass-dependent. As for *Saccharomyces cerevisiae*, although a reduction of 53.38% in lead biosorption was recorded due to methylation of amine groups, the drastic reduction by 96.34% when carboxylic acids was esterified, revealed that the carboxylic group contributed most significantly to lead biosorption.[51] Another research demonstrated that both modification of carboxylic and amine groups on the cell wall of *Saccharomyces cerevisiae* resulted in the decrease of biosorption capacity, but copper biosorption was more sensitive to modifications of the amine groups than of the carboxyl group.[52] On the other hand, Kılıç *et al.*[15] reported that carboxylic acids were more effective in Pb(II) sequestration while amine groups turned out to be more effective in Hg(II) sequestration. Seki *et al.*[53] showed that the interactions between the imidazol groups and the metal anions were relatively strong; however, the interactions between the amino groups and As(V) anions were very weak. Furthermore, Hydroxyl groups in the surface of *Penicillium cyclopium* were identified as providing the major

sites of heavy metal deposition, followed by amides and carboxylates. Phosphate groups and the lipids fraction of the biomass did not play significant role in biosorption of the metal ions in the studied biomass.[16] Carboxylate, amine and phosphate groups played an important role in the biosorption of metal ions by *Mucor rouxii* biomass.[9]

4. Conclusions

Results in this study showed the exact palladium uptake process, multi-scale visualization of palladium-loaded biomass and confirmed the contribution of functional groups to Pd(II) biosorption by *P. vermicola* biomass could be used as potential biosorbent for the recovery of Pd(II) from aqueous solutions (with an uptake of 115.79 mg g^{-1} under condition of pH 4, initial Pd(II) 200 mg L^{-1}, 30 °C). The pseudo-first order, pseudo-second order and intraparticle diffusion model indicated that chemical reaction was significant in the rate-controlling step and two steps governed adsorption rather than one. For equilibrium isotherms, Langmuir model fitted the Pd(II) adsorption data better than the Freundlich model, implying a monolayer adsorption trend. During the biosorption of palladium ions onto *P. vermicola*, the process is spontaneous and endothermic, and the randomness at the solid/liquid interface increases. SEM-EDX and TEM-EDX analyses identified that palladium ions were sorbed into both the external and internal of *P. vermicola* biomass, and the wt% of Pd and Cl in the surface of biomass reached 18.40% and 4.32%, respectively. As it was showed in AFM images, the morphologic properties of the palladium-loaded biomass changed considerably in the nanometer range. After sorbing Pd(II), *P. vermicola* biomass and nanoparticle aggregates coagulated together to form large clumps, which could attributed to the interactions between palladium ions and the surface of *P. vermicola* surface. In addition, the FTIR analysis indicated the involvement of N–H, O–H, –COOH, P=O and P–O in the sorption of Pd(II). The sorbed palladium ions were of zero-valent and divalent forms, and O, C, N and P atoms might possess sorption capabilities. By chemical modification, the spectral analysis and biosorption test disclosed that the decreasing contribution order of different functional groups in *P. vermicola* surface was carboxylic groups, hydroxyl groups, phosphate groups and amine groups, which caused about 40%, 40%, 10% and 10% reduction of palladium uptake. Future studies should focus on the industrial application of *P. vermicola* biomass by increasing the functional groups of surface through chemical or biological modification.

Acknowledgements

References

1 M. D. Yates, R. D. Cusick and B. E. Logan, *ACS Sustainable Chem. Eng.*, 2013, **1**, 1165–1171.

2 J. Park, S. W. Won, J. Mao, I. S. Kwak and Y. S. Yun, *J. Hazard. Mater.*, 2010, **181**, 794–800.

3 Q. Yi, R. Fan, F. Xie, Q. Zhang and Z. Luo, *J. Taiwan Inst. Chem. Eng.*, 2016, **61**, 299–305.

4 S. Morisada, Y. H. Kim, T. Ogata, Y. Marutani and Y. Nakano, *Ind. Eng. Chem. Res.*, 2011, **50**, 1875–1880.

5 S. W. Won, A. Lim and Y. S. Yun, *Bioresour. Technol.*, 2013, **137**, 400–403.

6 L. Le, H. Nan, D. Dexin, X. Xin, W. Yongdong, X. Jinhua, Z. Hui and T. Yan, *RSC Adv.*, 2015, **5**, 65827–65839.

7 I. Michalak, K. Chojnacka and A. Witek-Krowiak, *Appl. Biochem. Biotechnol.*, 2013, **170**, 1389–1416.

8 E. A. Dil, M. Ghaedi, G. R. Ghezelbash, A. Asfaram, A. M. Ghaedi and F. Mehrabi, *RSC Adv.*, 2016, **6**, 54149–54161.

9 G. Yan and T. Viraraghavan, *Eng. Life Sci.*, 2008, **8**, 363–371.

10 K. Chojnacka, A. Chojnacki and H. Gorecka, *Chemosphere*, 2005, **59**, 75–84.

11 S. W. Won, J. Mao, I. S. Kwak, M. Sathishkumar and Y. S. Yun, *Bioresour. Technol.*, 2010, **101**, 1135–1140.

12 A. E. Abo-Amer, A. B. Ramadan, M. Abo-State, M. A. Abu-Gharbia and H. E. Ahmed, *J. Basic Microbiol.*, 2013, **53**, 477–488.

13 S. Omeike, S. Kareem, S. Adewuyi and S. Balogun, *J. Life Sci.*, 2013, **15**, 119–124.

14 A. Kapoor and T. Viraraghavan, *Bioresour. Technol.*, 1997, **61**, 221–227.

15 M. Kılıç, M. E. Keskin, S. Mazlum and N. Mazlum, *Int. J. Miner. Process.*, 2008, **87**, 1–8.

16 K. Tsekova, D. Christova and M. Ianis, *Journal of Applied Sciences and Environmental Management*, 2006, **10**, 117–121.

17 J. Tobin, D. Cooper and R. Neufeld, *Enzyme Microb. Technol.*, 1990, **12**, 591–595.

18 J. Febrianto, A. N. Kosasih, J. Sunarso, Y. H. Ju, N. Indraswati and S. Ismadji, *J. Hazard. Mater.*, 2009, **162**, 616–645.

19 Y. S. Ho and G. McKay, *Process Biochem.*, 1999, **34**, 451–465.

20 W. J. Weber and J. C. Morris, *J. Sanit. Eng. Div., Am. Soc. Civ. Eng.*, 1963, **89**, 31–60.

21 A. E. Ofomaja, *Bioresour. Technol.*, 2010, **101**, 5868–5876.

22 M. Gan, S. Sun, Z. Zheng, H. Tang, J. Sheng, J. Zhu and X. Liu, *Appl. Surf. Sci.*, 2015, **356**, 986–997.

23 M. Gan, Z. Zheng, S. Sun, J. Zhu and X. Liu, *RSC Adv.*, 2015, **5**, 94500–94512.

24 A. E. Ofomaja, *Chem. Eng. J.*, 2008, **143**, 85–95.

25 Y. S. Ho and A. E. Ofomaja, *Biochem. Eng. J.*, 2006, **30**, 117–123.

26 M. Jain, V. Garg, U. Garg, K. Kadirvelu and M. Sillanpaa, *Int. J. Environ. Res.*, 2015, **9**, 1079–1088.

27 A. Sari, D. Mendil, M. Tuzen and M. Soylak, *J. Hazard. Mater.*, 2009, **162**, 874–879.

28 S. Kim, M. H. Song, W. Wei and Y. S. Yun, *J. Hazard. Mater.*, 2015, **283**, 657–662.

29 Z. Lin, J. Wu, R. Xue and Y. Yang, *Spectrochim. Acta, Part A*, 2005, **61**, 761–765.

30 J. Gardea-Torresdey, K. Tiemann, V. Armendariz, L. Bess-Oberto, R. Chianelli, J. Rios, J. Parsons and G. Gamez, *J. Hazard. Mater.*, 2000, **80**, 175–188.

31 M. Ghaedi, S. Hajati, F. Karimi, B. Barazesh and G. Ghezelbash, *J. Ind. Eng. Chem.*, 2013, **19**, 987–992.

32 H. Xie, Q. Zhao, Z. Zhou, Y. Wu, H. Wang and H. Xu, *RSC Adv.*, 2015, **5**, 33478–33488.

33 L. Ramrakhiani, R. Majumder and S. Khowala, *Chem. Eng. J.*, 2011, **171**, 1060–1068.

34 S. Srivastava and I. S. Thakur, *Curr. Microbiol.*, 2006, **53**, 232–237.

35 X. Li, C. Ding, J. Liao, L. Du, Q. Sun, J. Yang, Y. Yang, D. Zhang, J. Tang and N. Liu, *J. Environ. Sci.*, 2016, **41**, 162–171.

36 J. B. Omajali, I. P. Mikheenko, M. L. Merroun, J. Wood and L. E. Macaskie, *J. Nanopart. Res.*, 2015, **17**, 1–17.

37 K. Tamaoki, N. Saito, T. Nomura and Y. Konishi, *Hydrometallurgy*, 2013, **139**, 26–29.

38 P. K. Stoimenov, R. L. Klinger, G. L. Marchin and K. J. Klabunde, *Langmuir*, 2002, **18**, 6679–6686.

39 J. Pan, X. Ge, R. Liu and H. Tang, *Colloids Surf., B*, 2006, **52**, 89–95.

40 J. Bai, H. Yao, F. Fan, M. Lin, L. Zhang, H. Ding, F. Lei, X. Wu, X. Li and J. Guo, *J. Environ. Radioact.*, 2010, **101**, 969–973.

41 J. Jena, N. Pradhan, B. Dash, L. Sukla and P. Panda, *Int. J. Nanomater. Biostruct.*, 2013, **3**, 1–8.

42 Y. Yin, Y. Hu and F. Xiong, *Int. Biodeterior. Biodegrad.*, 2011, **65**, 1012–1018.

43 H. P. Song, X. G. Li, J. S. Sun, S. M. Xu and X. Han, *Chemosphere*, 2008, **72**, 616–621.

44 J. Wan, R. Ran, X. Wu, Y. Cao, M. Li, D. Weng and K. Huang, *Catal. Today*, 2015, **253**, 51–56.

45 S. Yang, J. Dong, Z. Yao, C. Shen, X. Shi, Y. Tian, S. Lin and X. Zhang, *Sci. Rep.*, 2014, **4**, 1–6.

46 J. Zhang, Y. Xu and B. Zhang, *Chem. Commun.*, 2014, **50**, 13451–13453.

47 H. Bubert, W. Brandl, S. Kittel, G. Marginean and D. Toma, *Anal. Bioanal. Chem.*, 2002, **374**, 1237–1241.

48 F. Ahimou, C. J. Boonaert, Y. Adriaensen, P. Jacques, P. Thonart, M. Paquot and P. G. Rouxhet, *J. Colloid Interface Sci.*, 2007, **309**, 49–55.

49 Y. Shen, T. Xiong, H. Du, H. Jin, J. Shang and K. Yang, *J. Sol-Gel Sci. Technol.*, 2009, **50**, 98–102.

50 W. Gao, B. Feng, Y. Ni, Y. Yang, X. Lu and J. Weng, *Appl. Surf. Sci.*, 2010, **257**, 538–546.

51 K. Parvathi, R. Nagendran and R. Nareshkumar, *Electron. J. Biotechnol.*, 2007, **10**, 92–105.

52 W. Jianlong, *Process Biochem.*, 2002, **37**, 847–850.

53 H. Seki, A. Suzuki and H. Maruyama, *J. Colloid Interface Sci.*, 2005, **281**, 261–266.